Improvements in the estimates of ice thickness and production in the Chukchi Sea polynyas derived from AMSR-E

Seelye Martin and Robert Drucker
School of Oceanography, University of Washington, Seattle, Washington, USA

Ronald Kwok and Benjamin Holt
Jet Propulsion Laboratory, California Institute of Technology, Pasadena, California, USA

Received 16 November 2004; revised 16 January 2005; accepted 7 February 2005; published 10 March 2005.

[1] For January–March 2003, we use 12.5-km resolution Advanced Microwave Scanning Radiometer (AMSR) data for the first time in a comparison with Synthetic Aperture Radar (SAR) and Special Sensor Microwave/Imager (SSM/I) data to study two Chukchi coast polynyas, one consisting of many, the other of only a few 25-km SSM/I pixels. Within these polynyas, the ice thicknesses are derived separately from the SMM/I 37-GHz and AMSR 36-GHz channels; the heat fluxes are derived by combining thicknesses with meteorological data. Comparison with ScanSAR data shows that for the large polynya, because AMSR provides better resolution of the surrounding coastline and first-year ice, the AMSR heat losses are greater than the SSM/I; for the small polynya, AMSR measures its variability even when its area is order of a single SSM/I pixel. This means that AMSR permits more accurate calculation of polynya heat losses, yielding the potential of improved estimates of Arctic polynya productivity. **Citation:** Martin, S., R. Drucker, R. Kwok, and B. Holt (2005), Improvements in the estimates of ice thickness and production in the Chukchi Sea polynyas derived from AMSR-E, *Geophys. Res. Lett.*, *32*, L05505, doi:10.1029/2004GL022013.

1. Introduction

[2] *Martin et al.* [2004] show that the thickness of thin ice can be derived from an algorithm based on the ratio of the Special Sensor Microwave/Imager (SSM/I) 37-GHz 25-km resolution vertical and horizontal brightness temperatures. For thicknesses less than 10 cm, the algorithm results compare well with thicknesses derived from clear-sky advanced very high resolution radiometer (AVHRR) data. For winter 2000 and the large coastal polynya that occurs along the Alaskan Chukchi coast between Cape Lisburne and Point Barrow, called here the Chukchi polynya, they further show that the thicknesses produced with this method can be combined with meteorological data and a heat flux model to provide daily and cumulative polynya heat losses.

[3] Although this SSM/I technique works well for the Chukchi polynya, *Winsor and Björk* [2000] show that out of approximately twenty-five Arctic Ocean polynyas, the Chukchi polynya is the largest. Of the remainder, about half are an order smaller and barely visible at the 25-km resolution. Because these smaller polynyas may be a large aggregate source of ice production, this suggests that the use of the polynya models based on SSM/I data alone will yield skewed estimates of the Arctic polynya ice production. The combined effect of the coarse SSM/I resolution and land-mask means that even for large polynyas such as the Chukchi, a fraction of the polynya can be obscured, while smaller polynyas can become invisible. The launch of the NASA AQUA satellite in 2002, with the Advanced Microwave Scanning Radiometer-EOS (AMSR-E, hereafter AMSR) provides an opportunity for improvement using the 12.5-km resolution AMSR 36-GHz channels.

[4] The question arises: why not use the 6.25-km resolution AMSR 89-GHz channel, instead of the 37-GHz to retrieve ice thickness? First, the 89-GHz channel is more sensitive than the 37-GHz to the water vapor generated by polynyas, so that 37 GHz should produce more accurate thicknesses. Second, the existing SSM/I 37 and 85 GHz algorithm of *Markus and Burns* [1995] classifies polynyas into open water, thin ice and first year ice, whereas *Martin et al.* [2004] yields thin ice thickness, which permits calculation of the heat loss.

[5] In the present paper, we adapt the SSM/I 37-GHz ice thickness algorithm to the AMSR 36-GHz channels, then for January–March 2003, use each instrument to examine the heat losses of two Alaskan coast Chukchi Sea polynyas. The first is the Chukchi polynya described above; the second is the much smaller polynya between Point Hope and Cape Lisburne, called here the Lisburne polynya. Figure 1 shows a map of the northwest Alaskan coast and the boxes outlining the location and maximum extent of these polynyas.

2. Adaptation of the SSM/I Ice Thickness Algorithm to AMSR

[6] As *Martin et al.* [2004] show, the thin ice thickness is a function of the brightness temperature ratio,

$$R_{37} = \frac{T_{B37V}}{T_{B37H}} \tag{1}$$

where the T_B are the SSM/I brightness temperatures, and the subscripts V and H refer to the vertical and horizontal brightnesses. If h_i is the ice thickness, this function has the following form:

$$h_i = \exp[1/(\alpha R_{37} + \beta)] - \gamma \tag{2}$$

where comparison with AVHRR yields that $\alpha = 230.5$, $\beta = -243.6$ and $\gamma = 1.008$. This curve is valid for $R_{37} < 1.4$, or

Copyright 2005 by the American Geophysical Union.
0094-8276/05/2004GL022013$05.00

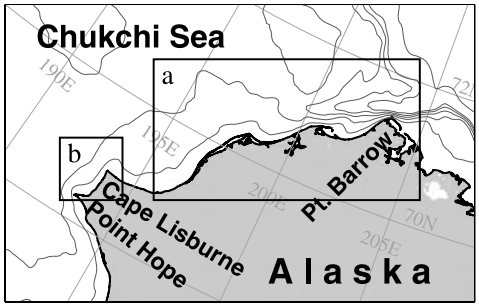

Figure 1. Map of the Alaskan Chukchi coast, showing the location of the boxes used in the analysis of the polynyas off (a) the Chukchi coast and (b) Cape Lisburne.

for minimum thicknesses of about 5 mm, and works best for thicknesses in the range 0.5 to 10 cm. Between 0.5 and 5 cm, the thicknesses have a standard deviation of about 1 cm, for thicknesses as large as 12 cm, the standard deviation is about 2 cm. In the following, we assume that the same algorithm can be used with the AMSR R_{36} ratio, where R_{36} is defined in an identical way to equation (1).

[7] Because of the seasonal drift of the AMSR data relative to the SSM/I, the AMSR and SSM/I data sets are cross-calibrated by first averaging the AMSR pixels to 25-km pixels coincident with the SSM/I grid. Then, for pixels from the entire Arctic Basin, we compare spatially coincident values of R_{36} and R_{37} in a daily scatterplot. In an example for January 18, 2003, Figure 2 shows that the two variables have a strong linear relation. Therefore we correct R_{36} to R_{37} using a daily linear regression. The advantage of this procedure is that equation (2) can be used with R_{36} without recalibration from visible/infrared imagery. For the first three months of 2003, the slope of the regression line varies between 1.07 and 1.17, and the intercept varies between −0.06 and −0.17. From the daily fit of R_{36} to R_{37}, the AMSR ice thicknesses are derived from equation (2), following which the heat fluxes through the ice are derived in an identical manner to *Martin et al.* [2004].

[8] In this procedure, the atmospheric heat flux is calculated using bulk coefficients from *Martin et al.* [1998], 2-m air temperatures from the 12-hr International Arctic Buoy Program (IABP) gridded data, and winds derived from the 6-hr National Center for Environmental Prediction (NCEP) surface level pressure gridded data. As *Martin et al.* [2004] justify, we assume that all of the polynya heat loss lies within the 10-cm ice thickness contour.

3. Land Contamination

[9] For coastal polynyas, the thinnest ice and largest heat fluxes occur within a few kilometers of land [*Pease*, 1987; *Martin*, 2002]. In our application of the algorithms to the polynya boxes in Figure 1, we next investigate whether only land needs to be masked, or if the row of oceanic pixels adjacent to land must also be masked. The effective fields-of-view of the SSM/I 37-GHz and AMSR 36-GHz channels are respectively 30 km × 37 km and 8 km × 14 km, with the main beam efficiency of the AMSR channel being slightly better (0.95) than the SSM/I (0.93) [*Martin*, 2004, chap. 8]. This means that the 25-km SSM/I and 12.5-km AMSR grid approximately match the effective instrument field-of-view, with some energy returned from outside the pixel. For the winter Ross Ice Shelf, *Jacobs and Comiso* [1989] show from the Scanning Multichannel Microwave Radiometer (SMMR) data, that the vertically polarized brightness temperatures for the shelf, sea ice and seawater lie in the range 190°–240°K. For this case when only moderate temperature differences exist among the surface types, their work suggests that adjacent to the shelf, the contributions external to the pixel in question can be ignored.

[10] For the Chukchi coast, examination of the regional winter brightness temperatures shows that for the two vertically polarized channels, the polynya, pack ice and land brightness temperatures are in the range 220°–250°K, while for the horizontally polarized temperatures are in the range 190°–225°K. Because the temperature differences among these surface types are small, the contamination from adjacent pixels at the transitions between these surfaces is also small. This means it is better to keep the pixels adjacent to land rather than to mask them. Further, for our study region, examination of several brightness temperature images taken under a variety of wind conditions shows that the oceanic brightness temperature changes adjacent to land are associated with opening and closing of the polynyas. Therefore, in each box and based on land boundary visible in the ScanSAR (Synthetic Aperture Radar) imagery, we mask only pixels containing land.

4. Comparison of the AMSR Heat Loss With ScanSAR Imagery

[11] For 18 January 2003 on the Alaskan Chukchi coast, Figure 3 compares the AMSR and SSM/I heat fluxes with a coincident ScanSAR image. For this day, the daily averaged winds over the region had offshore velocities of about 11 m s^{-1}, with air temperatures of about −21°C. Figure 3a shows the AMSR fluxes contoured over the ScanSAR image; Figures 3b and 3c show the AMSR and SSM/I heat fluxes in pixel form. For both cases, the pixels are restricted to ice thicknesses less than or equal to 10 cm. Because the

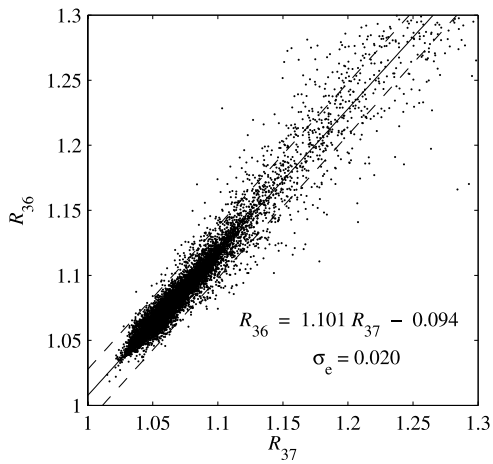

Figure 2. Scatterplot of AMSR R_{36} versus SSM/I R_{37} for January 18, 2003 and for the entire Arctic Basin. The solid line gives the best fit; the two dashed lines show the standard deviation of the error (σ_e).

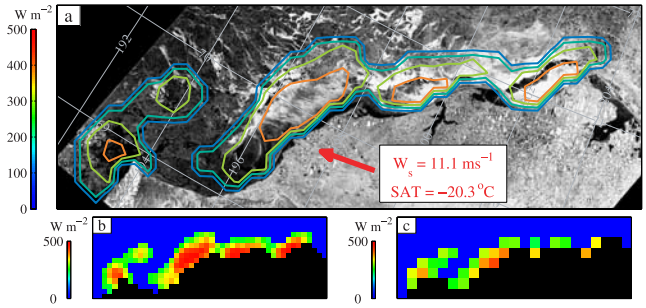

Figure 3. The AMSR and SSM/I derived heat fluxes for January 18, 2003. (a) Comparison of a ScanSAR image taken at 1726 UTC with the superimposed AMSR-derived daily averaged heat flux contours. The contours are at intervals of 100 W m^{-2}, where the red contour equals 400 W m^{-2}. The red arrow shows the wind direction, the inset box gives the daily averaged 2-m air temperature (SAT) and wind (W_s). (b) The pixel-by-pixel heat loss for AMSR and (c) SSM/I.

ScanSAR imagery is acquired at a specific time while the AMSR and SSM/I images are daily averages of ascending and descending orbits, the passive microwave and ScanSAR images differ slightly.

[12] On Figure 3a, the innermost red contour represents a heat loss of 400 W m^{-2}; the other colors represent smaller losses at intervals of 100 W m^{-2}. For the Chukchi polynya, the comparison shows that the largest heat losses occur in three locations, each corresponding to a bright region on the ScanSAR image. These bright regions consist of frazil and pancake ice that are organized into streaks by a wind- and wave-driven Langmuir circulation. The short waves accompanying the Langmuir circulation generate Bragg scattering that makes these regions appear bright. Because the ice in these regions is generally thin, it has large heat losses. Examination of the smaller Lisburne polynya shows that it is prominent in the AMSR heat flux but appears dark in the ScanSAR image; this may be because the polynya consists of thin flat ice instead of frazil ice. Comparison of Figures 3b and 3c shows that AMSR provides better definition of the polynyas than SSM/I. For Lisburne, the polynya core is described by about seven AMSR pixels but only one SSM/I pixel. For the Chukchi polynya, the ScanSAR and AMSR images show that the polynya consists of three well-defined small polynyas, whereas in the SSM/I, only the largest of the three is visible.

[13] Because of the increased resolution and the ability to use pixels closer to the coast, on this day, the total AMSR heat loss for the Chukchi polynya is 5.5 × 10^{17} J, compared with 3.0 × 10^{17} J for SSM/I, an 83% increase. For the Lisburne polynya, the AMSR heat loss is 1.2 × 10^{17} J compared with 1.0 × 10^{17} J for SSM/I, a 20% increase. For both polynyas, the increase in heat loss is associated with two factors, the improved AMSR land mask, and at the boundary between the polynya and the surrounding pack ice, the AMSR ability to resolve small areas of thin ice that in the corresponding SSM/I pixel might have thicknesses greater than 10 cm.

[14] Is the larger AMSR heat loss closer to the actual heat loss? In their comparison of the SSM/I heat flux algorithm against spatially averaged AVHRR estimates, *Martin et al.* [2004] describe how the presence of water vapor and low level clouds generated by polynyas makes it almost impossible to determine the total polynya heat loss with AVHRR. Instead, their AVHRR validation of the SSM/I algorithm was restricted to interior pixels that were nearly vapor free. Their pixel-by-pixel comparison shows that the accuracy of the SSM/I estimates is about ±80 W m^{-2} on typical losses of 300–400 W m^{-2} for a 20–25% error. If the AMSR algorithm has a similar accuracy, then the larger AMSR losses are associated with the better definition of the polynya area and are closer to the actual heat loss. Because of this water vapor problem, any absolute calibration of the total polynya heat loss will probably require low-level aircraft overflights.

[15] For 10 January 2003, an offshore surface wind of about 9 m s^{-1} and a 2-m air temperature of −18°C, Figure 4 compares AMSR, SSM/I and ScanSAR imagery of the Lisburne polynya. Figure 4a shows the AMSR heat flux contours superimposed on the ScanSAR image, where the inner contour corresponds to 300 W m^{-2}. Adjacent to the coast, the contours surround a region of frazil ice, with a less intense heat flux maximum offshore. Figures 4b and 4c respectively show the AMSR and SSM/I heat fluxes; the white square is missing data. Comparison of 4b and 4c show that similar to Figure 3, the polynya core is described by about seven AMSR pixels, but only one SSM/I pixel. For this day, the AMSR heat loss is 0.46 × 10^{17} J compared with an SSM/I value of 0.14 × 10^{17} J, so that the AMSR loss is more than three times the SSM/I.

5. Comparison of AMSR and SSM/I Cumulative Heat Losses

[16] For the first 90 days of 2003, Figure 5 compares for the two instruments and polynyas, the daily heat losses

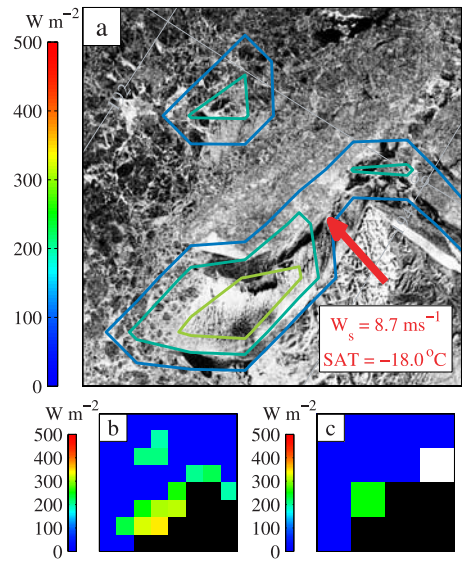

Figure 4. The AMSR and SSM/I derived heat fluxes for Cape Lisburne and January 10, 2003. (a) Comparison of a ScanSAR image taken at 1800 UTC with the superimposed AMSR-derived daily averaged heat flux contours. The innermost contour equals 300 W m^{-2}. (b) The pixel-by-pixel heat loss for AMSR and (c) SSM/I. See caption of Figure 3 for further description.

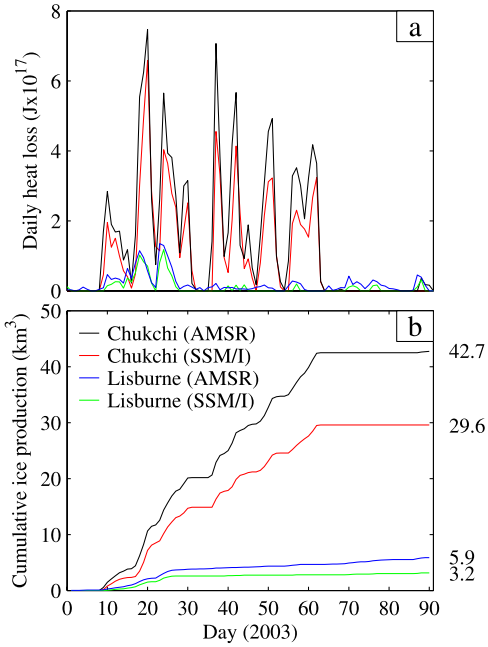

Figure 5. Comparison of (a) the daily polynya heat loss and (b) the cumulative ice production derived from SSM/I and AMSR data for the Chukchi and Lisburne polynyas, as identified by the different colors. The numbers to the right of 5b give the annual cumulative growth.

(Figure 5a) and the cumulative ice production (Figure 5b). In these calculations, we assume that the polynya activity begins in early January after the Chukchi Sea becomes ice covered. Figure 5a shows that the polynya heat losses exhibit the characteristic intermittency associated with the offshore wind variability. It also shows that for both polynyas, the AMSR heat losses are greater. For comparison with other investigators, Figure 5b presents the cumulative losses in units of km^3 of ice production. The figure shows that for the Chukchi polynya, the cumulative ice production is 29.6 km^3 for SSM/I and 42.7 km^3 for AMSR, a 44% increase. For the same polynya, *Martin et al.* [2004, Table 1] find from SSM/I for the period 1990–2001, an average ice production of 65 ± 43 km^3, and *Winsor and Chapman* [2002] find from a numerical model for 1990–1998, an average ice production of 67 ± 18 km^3. Both the 2003 AMSR and SSM/I Chukchi estimates are comparable with the earlier results. In contrast, the Lisburne polynya cumulative ice production is much smaller, being 3.2 km^3 for SSM/I and 5.9 km^3 for AMSR, an increase of 84%. This suggests that the effect of the AMSR resolution is more important for small polynyas.

6. Conclusions and Further Work

[17] The above work shows that the methods for estimating polynya heat loss developed by *Martin et al.* [2004] using the SSM/I R_{37}-ratio is adaptable to the AMSR 36-GHz channels. The AMSR resolution provides a significant increase in our ability to resolve the polynya areas and for our test areas, yields an increased polynya heat loss. This increase in heat loss is greatest for the small Lisburne polynya, with a smaller though significant increase for the larger Chukchi polynya. Given that many Arctic polynyas have sizes on the order of the Lisburne polynya, this means that AMSR has the potential to provide more accurate and larger estimates of the regional polynya productivity.

[18] **Acknowledgments.** SM and RD gratefully acknowledge the support of NASA under NAG5-11057. The JPL effort was supported by NASA through a contract with the Jet Propulsion Laboratory, California Institute of Technology. The authors thank Josefino Comiso for provision of the AMSR data. We also thank the National Snow and Ice Data Center in Boulder, CO for the SSM/I data and the Alaskan SAR Facility for the SAR data. SAR images copyright Canadian Space Agency 2003.

References

Jacobs, S. S., and J. C. Comiso (1989), Sea ice and oceanic processes on the Ross Sea continental shelf, *J. Geophys. Res.*, *94*, 18,195–18,211.
Markus, T., and B. A. Burns (1995), A method to estimate sub-pixel scale coastal polynyas with satellite passive microwave data, *J. Geophys. Res.*, *100*, 4473–4487.
Martin, S. (2002), Polynyas, in *Encyclopedia of Ocean Sciences*, edited by J. H. Steele, K. K. Turekian, and S. A. Thorpe, pp. 2241–2247, Elsevier, New York.
Martin, S. (2004), *An Introduction to Ocean Remote Sensing*, Cambridge Univ. Press, New York.
Martin, S., R. Drucker, and K. Yamashita (1998), The production of ice and dense shelf water in the Okhotsk Sea polynyas, *J. Geophys. Res.*, *103*, 27,771–27,782.
Martin, S., R. Drucker, R. Kwok, and B. Holt (2004), Estimation of the thin ice thickness and heat flux for the Chukchi Sea Alaskan coast polynya from SSM/I data, 1990–2001, *J. Geophys. Res.*, *109*, C10012, doi:10.1029/2004JC002428.
Pease, C. H. (1987), The size of wind-driven coastal polynyas, *J. Geophys. Res.*, *92*, 7049–7059.
Winsor, P., and G. Björk (2000), Polynya activity in the Arctic Ocean from 1958 to 1997, *J. Geophys. Res.*, *105*, 8789–8803.
Winsor, P., and D. C. Chapman (2002), Distribution and interannual variability of dense water production from coastal polynyas on the Chukchi Shelf, *J. Geophys. Res.*, *107*(C7), 3079, doi:10.1029/2001JC000984.

R. Drucker and S. Martin, School of Oceanography, University of Washington, Box 357940, Seattle, WA 98195-7940, USA. (seelye@ocean.washington.edu)
B. Holt and R. Kwok, Jet Propulsion Laboratory, California Institute of Technology, 4800 Oak Grove Drive, Pasadena, CA 91109, USA.